Modeling the Interaction between Quasigeostrophic Vertical Motion and Convection in a Single Column

JI NIE

Lamont-Doherty Earth Observatory, Columbia University, New York, New York

ADAM H. SOBEL

Department of Applied Physics and Applied Mathematics, and Lamont-Doherty Earth Observatory, Columbia University, New York, New York

(Manuscript received 18 July 2015, in final form 1 December 2015)

ABSTRACT

A single-column modeling approach is proposed to study the interaction between convection and large-scale dynamics using the quasigeostrophic (QG) framework. This approach extends the notion of ''parameterization of large-scale dynamics,'' previously applied in the tropics via the weak temperature gradient approximation and other comparable methods, to the extratropics, where balanced adiabatic dynamics plays a larger role in inducing large-scale vertical motion. The diabatic heating in an air column is resolved numerically by a single-column model or a cloud-resolving model. The large-scale vertical velocity, which controls vertical advection of temperature and moisture, is computed through the QG omega equation including the dry adiabatic terms and the diabatic heating term. The component due to diabatic heating can be thought of as geostrophic adjustment to that heating and couples the convection to the large-scale vertical motion. The approach is demonstrated using two representations of convection: a single-column model and linear response functions derived by Z. Kuang from a large set of cloud-resolving simulations. The results are qualitatively similar in both cases. The behavior of convection that is strongly coupled to large-scale dynamics is significantly different from that in the uncoupled case. The positive feedback of the diabatic heating on the large-scale vertical motion reduces the stability of the system, extends the decay time scale after initial perturbations, and increases the amplitude of convective responses to transient large-scale perturbations or imposed forcings. The diabatic feedback of convection on vertical motion is strongest for horizontal wavelengths on the order of the Rossby deformation radius.

1. Introduction

There has been steady development in tropical meteorology in recent years in the modeling of convection, in either a single column or a limited domain with periodic horizontal boundaries, with the large-scale dynamical tendencies parameterized, rather than being either neglected or externally imposed. These ideas, namely the weak temperature gradient approximation (WTG; Sobel and Bretherton 2000; Raymond and Zeng 2005; Wang and Sobel 2011), the damped gravity wave method (Kuang 2008; Blossey et al. 2009; Romps 2012a,b), as well as other related ones (e.g., Mapes 2004; Bergman and Sardeshmukh 2004), parameterize the ''supradomain-scale'' vertical motion as functions of the state variables of the local air column and prescribed parameters of the large-scale environment. These approaches have been applied to multiple topics in tropical meteorology, such as the responses of convection to remote SST anomalies (e.g., Chiang and Sobel 2002), to stratospheric perturbations such as those associated with the quasi-biennial oscillation (Nie and Sobel 2015), to convectively coupled waves (e.g., Kuang 2008, 2012), and to convection–radiation interaction (e.g., Sobel et al. 2007; Emanuel et al. 2014).

Having been developed for the tropics, all of these approaches neglect the influence of large-scale quasi-balanced dynamics, such as that associated with the advection of potential vorticity anomalies along potential temperature surfaces (e.g., Hoskins et al. 1983), in causing large-scale vertical motion. As a consequence,

Corresponding author address: Ji Nie, Lamont-Doherty Earth Observatory, 301E Oceanography, 61 Route 9W, Palisades, NY 10964.
E-mail: jn2460@columbia.edu

DOI: 10.1175/JAS-D-15-0205.1

none of them is applicable to the extratropics, where such dry adiabatic dynamical processes cannot be ignored.

The purpose of this paper is to develop a parameterization of large-scale dynamics that can be used in the extratropics, including dynamical forcing of vertical motion by balanced disturbances. We choose to do this within the framework of the quasigeostrophic (QG) omega equation, arguably the simplest framework in which to adopt this idea. As in WTG and the other tropical approaches cited above, our modeling object is a single atmospheric column, and the large-scale flow is not explicitly resolved. Horizontal advective tendencies are prescribed, while large-scale vertical motion is parameterized. When coupled with the QG system, convection in the column is influenced by vertical motion due to the dry QG forcing (through the influence of that vertical motion on atmospheric state variables: temperature and moisture) but also can induce vertical motion associated with geostrophic adjustment to convective heating, thus feeding back to the QG vertical motion.

We call this modeling framework the column QG (CQG) framework, since it models the states of an atmospheric column under QG dynamics. Compared to conventional single-column modeling approaches in which the large-scale vertical motion is prescribed and largely determines local convection, the CQG approach calculates diabatic heating and the associated vertical motion interactively based on the evolving states of the air column. CQG allows us to attribute precipitation variations to different large-scale forcings and the associated convective feedback. With these features, CQG can be a useful tool to study the coupling between convection and large-scale dynamics outside the deep tropics. It is particularly relevant for disturbances in which convection and associated latent heating are strong, but dry adiabatic dynamics are as well. Many extreme precipitation events in the subtropics and extratropics fit this description.

This paper is organized as the following: after introducing the CQG framework (section 2) and the numerical methods (section 3), we explore its basic properties by examining its responses to both initial perturbations and imposed forcings (section 4), using both a single-column model with a convective parameterization and a linear response matrix (Kuang 2010) to represent the convective physics. In this paper, we shall limit ourselves to small perturbations in the linear regime as a first attempt. As will be seen, when coupled with the QG vertical motion, convection shows intriguing responses that are significantly different from convection that is decoupled with large-scale dynamics. Using the convective linear response matrix, we discretize the full CQG system into a linear matrix system and gain insights of the dependencies of its dynamics on the length scale of the system using eigenanalysis. Discussion is in section 5, followed by a summary of our main conclusions (section 6).

2. Formulation

The modeling object in the CQG framework is an air column with the size of a typical GCM grid. Its temperature T and specific humidity q equations in pressure p coordinates may be written as

$$\partial_t T = \mathrm{Adv}_T + \frac{\sigma p}{R}\omega + Q \quad \text{and} \tag{1}$$

$$\partial_t q = \mathrm{Adv}_q - s_q\omega + Q_q, \tag{2}$$

where $\sigma = -(RT/p)\partial_p \ln\theta$ is the static stability and $s_q = \partial_p q$. The term ω is the pressure velocity. The large-scale horizontal temperature and moisture advection are Adv_T and Adv_q, respectively, where $\mathrm{Adv}_* = -(u\partial_x + v\partial_y)$. The terms Q and Q_q are the convective heating and moistening tendencies, respectively. Because radiative cooling is fixed in this study, the radiative cooling in the temperature equation is absorbed into Q. One can easily write the radiative cooling separately in Eq. (1) if radiation is relevant in the dynamics.

The convective-scale processes within the column can be represented numerically by a single-column model (SCM) or a cloud-resolving model (CRM), providing the Q and Q_q terms in the above equations. If the horizontal advection terms are viewed as external forcing, then the only quantity needed to fully specify the system is ω. However, the vertical advection terms, containing ω, are often dominant in the temperature and moisture equations. In simulations of convection in a single-column or limited domain, the occurrence and intensity of convection are largely determined by how ω is specified.

In the QG dynamical system, the vertical motion ω can be diagnosed instantaneously (i.e., without time derivatives) using the QGω equation [e.g., Eq. (6.34) in Holton (2004, 164–168)]:

$$\partial_{pp}\omega + \frac{\sigma}{f_0^2}\nabla^2\omega = -\frac{1}{f_0}\partial_p \mathrm{Adv}_\zeta - \frac{R}{pf_0^2}\nabla^2 \mathrm{Adv}_T - \frac{R}{pf_0^2}\nabla^2 Q, \tag{3}$$

where $\zeta = (1/f_0)\nabla^2\phi + f$ is the total vorticity, ϕ is geopotential height, and f_0 is the reference value of the Coriolis parameter. The notation ∇^2 refers to the horizontal Laplacian operator, $\nabla^2 = (\partial_{xx} + \partial_{yy})$. The right-hand-side (rhs) terms are the vertical derivative of the horizontal advection of total vorticity (referred as vorticity advection), the horizontal Laplacian of the horizontal differential advection of temperature, and the

diabatic heating term, respectively. Equation (3) is a linear equation, so it can be solved including the rhs terms one by one. Assuming $\omega = 0$ at the upper and lower boundaries, ω can be decomposed into three components:

$$\omega = \omega_\zeta + \omega_T + \omega_Q, \tag{4}$$

where ω_ζ is the component of vertical motion due to the vorticity advection only [i.e., the solution of Eq. (3) with only the first term on the rhs]. Analogously, ω_T and ω_Q are the components of vertical motion due to the temperature advection and the diabatic heating, respectively. There are several other alternative formulations of the QGω equation, such as the **Q**-vector formulation (Hoskins et al. 1978) and Trenberth's formulation (Trenberth 1978). The CQG framework presented here does not require any particular formulation as long as the diabatic component ω_Q is retained in the QGω equation.

For extratropical atmospheric disturbances, the relative importance of ω_ζ, ω_T, and ω_Q are strongly related to the length scale of the disturbance in question. Assuming that a disturbance has a characteristic wavelength L, corresponding to wavenumber $k = 2\pi/L$, the QGω equation for the single wavenumber is

$$\partial_{pp}\omega - \sigma\left(\frac{k}{f_0}\right)^2\omega = -\frac{1}{f_0}\partial_p \mathrm{Adv}_\zeta + \frac{R}{p}\left(\frac{k}{f_0}\right)^2 \mathrm{Adv}_T + \frac{R}{p}\left(\frac{k}{f_0}\right)^2 Q. \tag{5}$$

The Rossby radius of deformation in our pressure coordinate is $L_R = (\sqrt{\sigma}\Delta P)/f_0$, where ΔP is a representative vertical scale of the motion in pressure. If we multiply the entire Eq. (5) by the constant ΔP^2, we see that the coefficient on the second term on the lhs becomes $k^2 L_R^2$, the ratio of the deformation radius to the horizontal scale of the motion. The latter two terms on the rhs also then contain this coefficient, though multiplied by the nondimensional constant $(R\Delta P^2)/(\sigma p)$. Thus, as can be seen from Eq. (5), when the length scale of the disturbance is large compared to the Rossby radius of deformation, the balance is between the first term on the lhs and the first on the rhs, so that ω is determined mainly by the vorticity advection. In this case, convection and large-scale dynamics are decoupled: convection feels the effects of the large-scale ω induced by the vorticity advection but does not feed back to ω. This longwave limit is equivalent to imposing large-scale total ω. On the other hand, when the length scale is small compared to the deformation radius, the first terms on the lhs and rhs become small compared to the others. In this limit, ω is mainly determined by the temperature advection and the diabatic heating. Though not apparent from Eq. (5) alone, the horizontal temperature advection also becomes small in this limit by standard scaling arguments (e.g., Charney 1963; Sobel et al. 2001). Thus, as f_0 approaches zero, the QGω equation approaches the strict WTG formulation, in which diabatic heating alone determines the vertical motion (Sobel and Bretherton 2000).

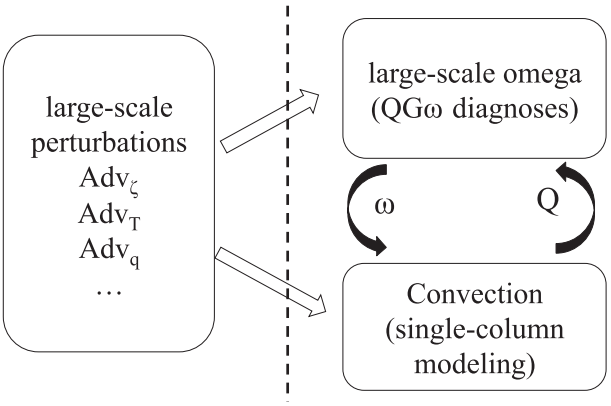

FIG. 1. A schematic of the CQG modeling framework. See text for details.

Convection in the longwave (imposed ω) and short wave (WTG) limits has been investigated by many previous studies. The regime of our primary interest here, on the other hand, is convection associated with disturbances whose wavelengths are on the order of the deformation radius. For typical parameter values in the subtropics and midlatitudes, $L_R \sim 1000$ km, and the length scales of interest range from several hundred to several thousand kilometers. Over this range, both the vertical motion forced by dry dynamics $\omega_\zeta + \omega_T$ and that due to convective heating ω_Q may play important roles in the system. This regime may be relevant, for example, to many extreme precipitation events outside the deep tropics. Synoptic-scale forcing plays an important role in many such events, but deep convection is typically also strong, perhaps dominant in the thermodynamic equations, so that a thorough understanding of such events requires a way to analyze the coupling between the two sets of processes.

The CQG modeling framework is simply the modeling of convection in a single column [Eqs. (1) and (2)] and the QG vertical motion together using the QGω equation [Eq. (5)]. A schematic of the framework is shown in Fig. 1. The convective processes within the column are numerically represented by an SCM or a CRM. The column feels the effects of ω through the associated vertical advection of potential temperature and moisture, and the convection feeds back to ω through diabatic heating ω_Q and indirectly through Q_q in the moisture equation. The strength of the coupling is set by the wavenumber k (or, equivalently, wavelength L). The

vertical dashed line in Fig. 1 separates the internal components of the CQG convective system to the right and the external perturbations to the left. The external large-scale perturbations include Adv_ζ, Adv_T, and Adv_q as marked in Fig. 1 and others unmarked such as topography-forced vertical motion and sea surface temperature (SST) forcing. Different types of forcing may have different pathways to enter the CQG system, as denoted by the arrows crossing the vertical dashed line. The vorticity advection Adv_ζ dynamically forces ω_ζ. The temperature advection Adv_T has both a dynamical effect through the omega equation and a thermodynamic effect through the temperature equation. The term Adv_q has only a thermodynamic effect, through the moisture equation.

A significant limitation is that we view the large-scale dynamical forcings, Adv_ζ, Adv_T, and Adv_q, as external and given. In reality, convection can alter the large-scale disturbances responsible for these forcings. It is impossible to include all the processes of the three-dimensional atmosphere in a one-dimensional system, so that some compromise is unavoidable in any approach that makes such a reduction. We view ours as a reasonable compromise, whose consequences need to be explored by experimentation.

3. Numerical methods

a. Single-column model

Two representations of convection are used to calculate the convective tendencies. The first is the MIT single-column model (Emanuel and Živkovic-Rothman 1999). It applies a buoyancy sorting convection scheme (Emanuel 1991) that represents an entire spectrum of convective clouds, as well as a stratiform cloud parameterization (Bony and Emanuel 2001). The surface fluxes are calculated from simple aerodynamic flux formulae with fixed surface wind of $5\,\mathrm{m\,s^{-1}}$ augmented by convective gusts. An ocean surface with fixed SST of 300 K is the lower boundary. An idealized radiative cooling (Pauluis and Garner 2006) is applied, specified to be $-1.5\,\mathrm{K\,day^{-1}}$ in the troposphere and relaxation of the temperature toward 200 K with a 5-day time scale in the stratosphere. The SCM is run with a vertical resolution of 25 hPa and a time step of 5 min.

The upper- and lower-boundary conditions for the QGω equation are $\omega = 0$ at the nominal tropopause, specified to be 175 hPa, and the top of the planetary boundary layer (PBL) specified to be 900 hPa. Results are not sensitive to reasonable changes of the heights of the upper and lower boundaries. In our simulations with the SCM, σ is calculated from the temperature profile and updated with time. In our simulations with the linear response function (LRF), σ is calculated from the reference temperature profile in steady state. For the small perturbations examined here, the effect of including σ perturbations is negligible. A key control parameter in the QGω equation is k/f_0, corresponding to the nondimensional parameter $k^2L_R^2$. We fix f_0 to be $7\times10^{-5}\,\mathrm{rad\,s^{-1}}$, which is close to its value at 30°N. The static stability σ is not taken constant with height here, but a representative value is $2\times10^{-6}\,\mathrm{m^2\,Pa^{-2}\,s^{-2}}$. For a pressure depth scale on the order of the depth of the troposphere, this yields $L_R \sim 2000$ km. Accordingly, we vary k between values corresponding to wavelengths from 10 000 to 500 km. For wavelengths much smaller than 500 km, the QG approximation ceases to hold to a useful degree of approximation.

The SCM is initialized with the sounding profiles of the radiative–convective equilibrium (RCE) state. These are determined by an initial simulation period in which we impose $\omega = 0$ at all levels and allow the model to come to equilibrium. After this, the SCM is coupled to ω as computed by Eq. (5), but without any forcing imposed, and again allow equilibrium to be reached. As we will argue in section 3, the model will reach a steady state that has the same T and q with the RCE state and time-mean ω of zero. Then, at a time that we call day 0, initial perturbations or forcings are imposed on the SCM while keeping convection coupled to ω. In this study, we only consider small perturbations or forcings, thus viewing Eqs. (1), (2), and (5) as governing perturbations from the RCE reference state. The deviation symbol ($'$) is, however, omitted in the following equations for simplicity.

b. Convective-response-functions approach

In addition to the SCM, a set of convective LRFs (Kuang 2010) is used in a separate set of calculations as the convective closure. Kuang (2010) pointed out that the responses of an ensemble of convective clouds to sizable temperature and moisture perturbations can be quite linear, although the processes involved in individual clouds are highly nonlinear. He suggested that a linear matrix might be sufficient to describe the anomalous convective tendencies around a reference state:

$$\begin{bmatrix} Q \\ Q_q \end{bmatrix} = \begin{bmatrix} \mathbf{M}_1 & \mathbf{M}_2 \\ \mathbf{M}_3 & \mathbf{M}_4 \end{bmatrix} \times \begin{bmatrix} T \\ q \end{bmatrix}, \tag{6}$$

where $\mathbf{M}_1$–$\mathbf{M}_4$ are the LRF matrices that represent anomalous convective heating (moistening) tendencies to temperature (moisture) anomalies, respectively. For example, each column in $\mathbf{M}_1$ indicates the anomalous convective heating tendencies at all levels in response to a unit temperature anomaly at the single level

corresponding to that column's location along the row of the matrix.

Although the construction of the LRF requires a large amount of computation, it condenses all the complexities of convective-scale processes into a matrix whose subsequent application is then extremely computationally cheap. The LRF can be used as a phenomenological but relatively accurate convective closure for idealized models—for example, models of convectively coupled waves (Kuang 2010) and of idealized Walker circulations (Kuang 2012). In the above two studies, the results using LRF match the results using the full CRM quite well.

The LRF matrix used in this paper is the one in Kuang (2012; the "28-layer 128-km case" of "unorganized" convection). It is constructed based on CRM runs in a domain of 128 km × 128 km × 32 km with 2-km horizontal resolution and 28 vertical levels. The reference state is an RCE state over a fixed SST of 300 K with the same radiation treatment as in the SCM simulations. The CRM uses a bulk aerodynamic formula with a constant 10-m exchange coefficient of 10^{-3} and a constant surface wind speed of 5 m s^{-1}.

Adopting the LRF approach benefits the current study in two ways. It provides a convective closure that is based on the CRM physics independent from the SCM. For small perturbations around the reference state, the LRF represents convection with the fidelity close to that of the CRM. Thus, results using the LRF may serve as a benchmark for those using the SCM and help identify the deficiencies of the convective parameterization in the SCM. Besides, as will see in section 4b, by using the LRF, we can describe the entire CQG system by a single linear matrix system and explore its dynamics with eigenanalysis.

4. Results

We start by considering the simplest case: the steady state of the CQG system. Before making the steady-state assumption or any other additional approximation, we can combine Eqs. (1) and (5) to eliminate the diabatic heating term, obtaining the following equation:

$$\partial_{pp}\omega = -\frac{1}{f_0}\partial_p \mathrm{Adv}_\zeta + \frac{Rk^2}{pf_0^2}\partial_t T. \tag{7}$$

While this negates the purpose of the ω equation by reintroducing a time derivative, it is useful in that it allows us to see a basic property of the CQG system. Equation (7) shows that in steady state ($\partial_t T = 0$), a nonzero ω can be forced dynamically (by Adv_ζ) but not thermodynamically (by Adv_T or Adv_q). Thermodynamic advective forcings still have an impact, in that the steady state requires convective heating and moistening anomalies to exactly balance those forcings. Those convective tendency anomalies are in turn associated with corresponding temperature and moisture anomalies. Another property demonstrated by Eq. (7) is that steady states are independent of wavenumber k. These statements involve nothing about convective dynamics and have to be satisfied unless a steady state cannot be reached. Our numerical simulations with either the SCM or the LRF do reach steady states in the absence of time-dependent boundary conditions or forcings and confirm the above statements (not shown). The results with the SCM and with the LRF agree with each other quite well. Nonsteady-state solutions in the force-free cases may exist by, for example, allowing cloud–radiation interactions or starting with particular initial conditions. Those possibilities, however, are not explored in this paper.

The steady-state solution is a useful reference point, but any truly steady forcing—for example, due to the time-mean large-scale circulation and responses to it—are better absorbed into the reference state. The CQG framework is likely to be more useful for investigating responses to time-dependent forcing, for example, due to synoptic-scale disturbances in the extratropics. Thus, in this section we mainly focus on the transient behavior of the CQG system.

a. *Responses to initial perturbations*

We start by examining how convection responds to initial temperature and moisture perturbations in the absence of large-scale vertical motion, as in several previous studies (e.g., Kuang 2010; Tulich and Mapes 2010; Nie and Kuang 2012a,b). This uncoupled setting will form our baseline, against which we will then compare convection coupled to large-scale vertical motion under the CQG framework.

As an example, the evolution of convection in the CQG framework after introduction of an initial specific humidity perturbation in the middle troposphere is shown in Figs. 2–4. Figure 2 contains results with L = 10 000 km, which is essentially the case in which convection is decoupled from large-scale ω. All horizontal advective forcings are set to zero in these simulations. The results with the LRF (Figs. 2a,b) are very close to those shown in Kuang (2010, their Fig. A4, which shows only the first 12 h). The moisture perturbation is damped through convective adjustment, decreasing by about half its initial amplitude in the first 12 h. The moisture anomaly favors deep convection, leading to warm temperature anomalies at and above the perturbed layer and cold and dry anomalies below. The results with the SCM (Figs. 2c,d) are qualitatively

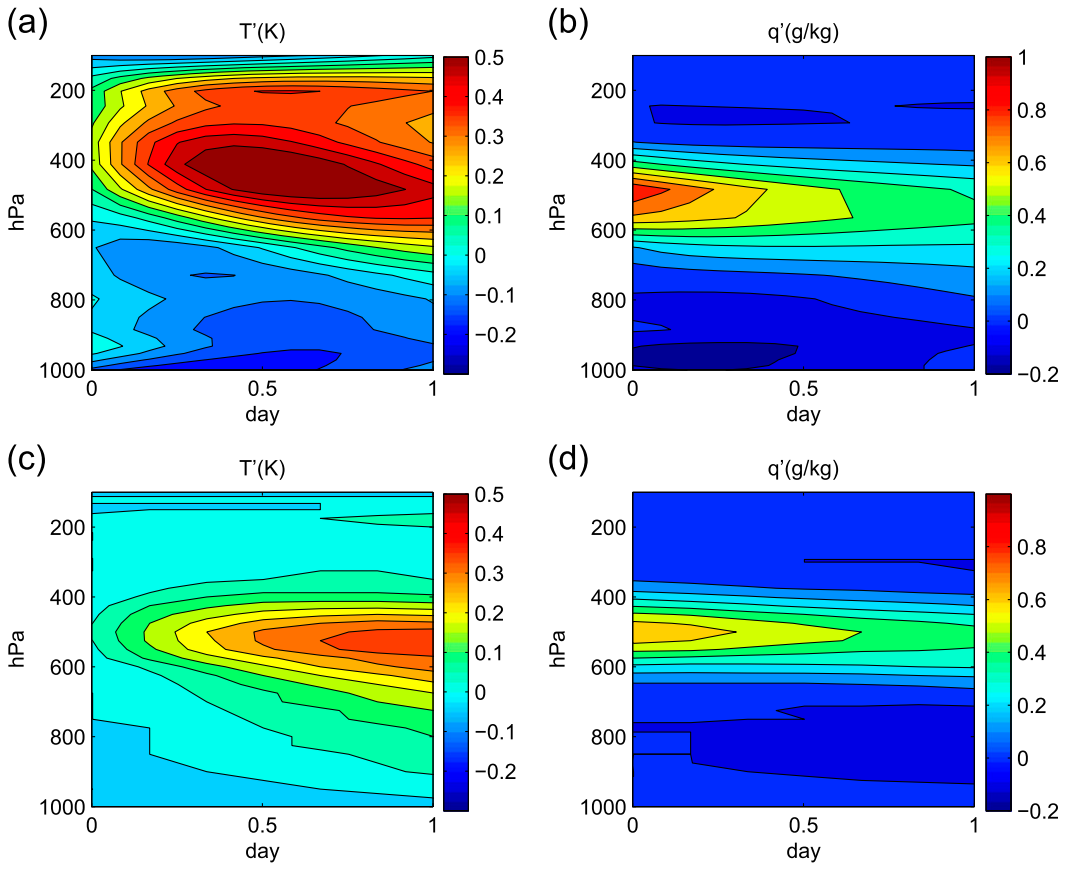

FIG. 2. Time series of (a),(c) temperature and (b),(d) specific humidity anomalies after an initial specific humidity perturbation is introduced at 500 hPa for the $L = 10\,000$-km case. The specific humidity perturbation is Gaussian shaped with a standard deviation of 75 hPa and an amplitude of 1 g kg^{-1}. (top) Results with the LRF and (bottom) results with the SCM. The ω response is very close to zero, thus omitted in the figure.

similar to the results with the LRF, capturing the damping of the moisture anomaly and warming of the middle troposphere. The differences between the two may be viewed as a manifestation of the differences between the response functions of the SCM and the CRM, though we do not explicitly calculate the SCM response functions. The SCM has a weaker response to moisture perturbations than does the LRF and a response more localized in and near the perturbed layer (Herman and Kuang 2013). These discrepancies between convective responses of the SCM and the LRF are consistent with the delay of the middle-troposphere warming and lack of cooling in the lower troposphere as seen in Fig. 2c. The precipitation anomaly with the SCM shows an oscillation with longer period and weaker damping than that with the LRF (comparing red lines in Fig. 4d and Fig. 3d).

Figure 3 and Fig. 4 show the responses to the same perturbation but with $L = 1000$ km. The results in Fig. 3 are from the LRF and those in Fig. 4 from the SCM. Now strongly coupled with QG ω, the responses of convection are significantly different from the decoupled case shown in Fig. 2. Initially, the moisture anomaly also leads to anomalous convective heating at and above the perturbed layer and cooling below (Fig. 3a). The anomalous heating and cooling excite strong upward motion in the upper troposphere and downward motion in the lower troposphere (Fig. 3c) through the QGω equation. The diabatic-heating-forced upward motion is associated with adiabatic cooling that partly cancels the diabatic heating. The upward motion also transports moisture vertically, replenishing the decaying moisture anomalies (Fig. 3b). Both of the temperature and moisture effects of ω make the convective adjustment less effective at damping the initial perturbation and lead to a longer response time. The ω, temperature, and moisture anomalies also propagate downward over a time scale of about 6 days. A comparison of the precipitation anomalies between the $L = 1000$-km and the $L = 10\,000$-km cases (Fig. 3d) highlights the extension of convective-response time when coupled with ω. The accumulated anomalous precipitation (e.g., within

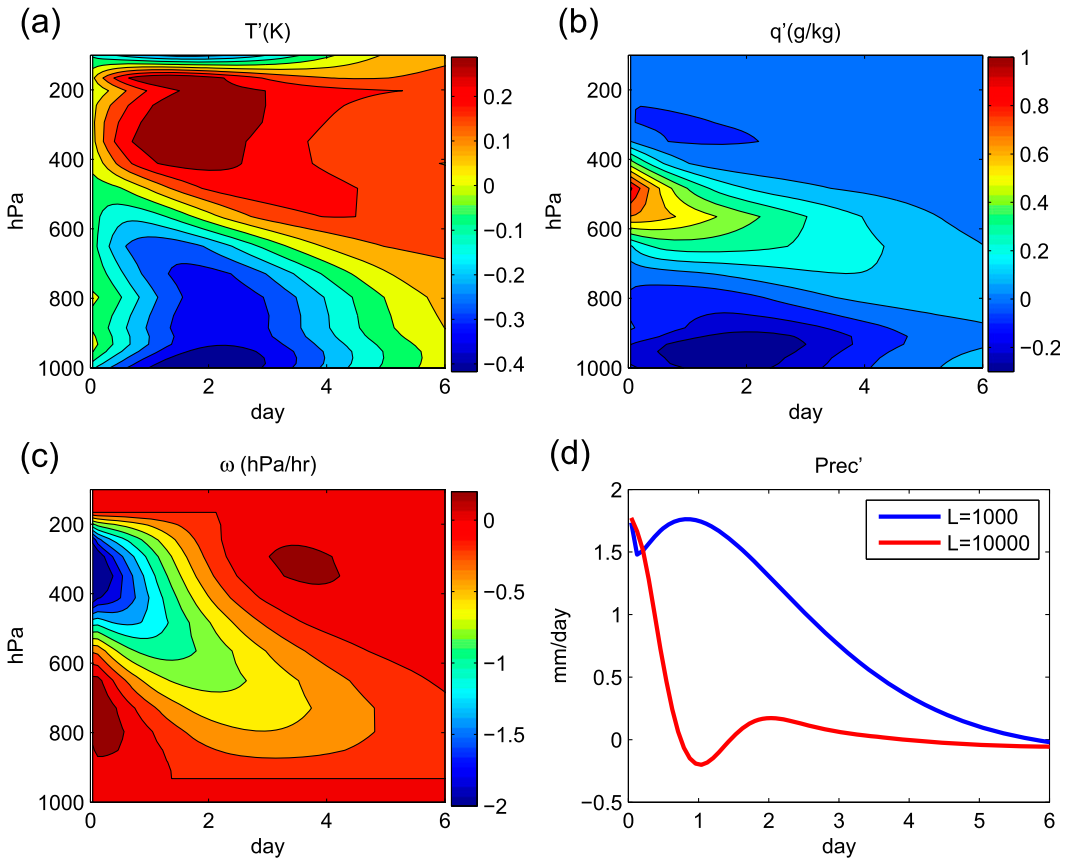

FIG. 3. Time series of (a) temperature, (b) specific humidity, (c) ω, and (d) precipitation anomalies with the same moisture perturbation as in Fig. 2. These are the results for the $L = 1000$-km case using the LRF. In (c), $\omega = \omega_Q$ in the absence of Adv_ζ and Adv_T. In (d), the precipitation anomaly in the $L = 10\,000$-km case is also shown as the red line.

6 days) is significantly larger in the $L = 1000$-km case than that in the $L = 10\,000$-km case.

The SCM results (Fig. 4) again are largely similar to the LRF results. The main features, such as the upward ω and the downward propagation of the signals are well captured by the SCM results. The response time seen from precipitation (Fig. 4d; e.g., the time at which the precipitation anomaly first reaches zero) is also longer in the coupled case (about 6 days) than in the decoupled case (about 1.5 days). The enhancement of precipitation anomalies is mostly due to the adiabatic cooling associated with the diabatic-heating-induced upward ω. The surface heat flux anomalies are very small, and their contribution to the precipitation anomalies is negligible. However, there are discrepancies between the results with the LRF and those with the SCM, mainly in the temperature responses. The amplitude of the response in the SCM results is also smaller than that in the LRF results. These discrepancies are due to the different representations of convection by different models. The effects of coupling convection to the QG dynamics in the CQG framework, however, are similar in the two cases.

We have also examined the responses of convection to initial temperature and moisture perturbations at other vertical levels (figures are not shown). For the decoupled convection, the results are very close to those in Kuang (2010). When convection is strongly coupled with QG ω (e.g., $L = 1000$ km), on the other hand, the diabatic-heating-induced ω plays a significant role and the response time is extended to several days as shown in Figs. 3 and 4.

The dependence of the response time scale on L may be understood by the following qualitative argument. In Eq. (7), the eigenmodes of the lhs operator are sinusoids in the vertical direction. In the absence of advective forcing, projecting all variables on the sinusoidal eigenmodes and approximating the coefficients (e.g., p and σ) as constants, Eq. (7) becomes

$$-m^2 w_m = \frac{R}{p f_0^2} k^2 \partial_t T_m, \tag{8}$$

where the subscript denotes projection on mode m. Plugging Eq. (8) into Eq. (1), one has

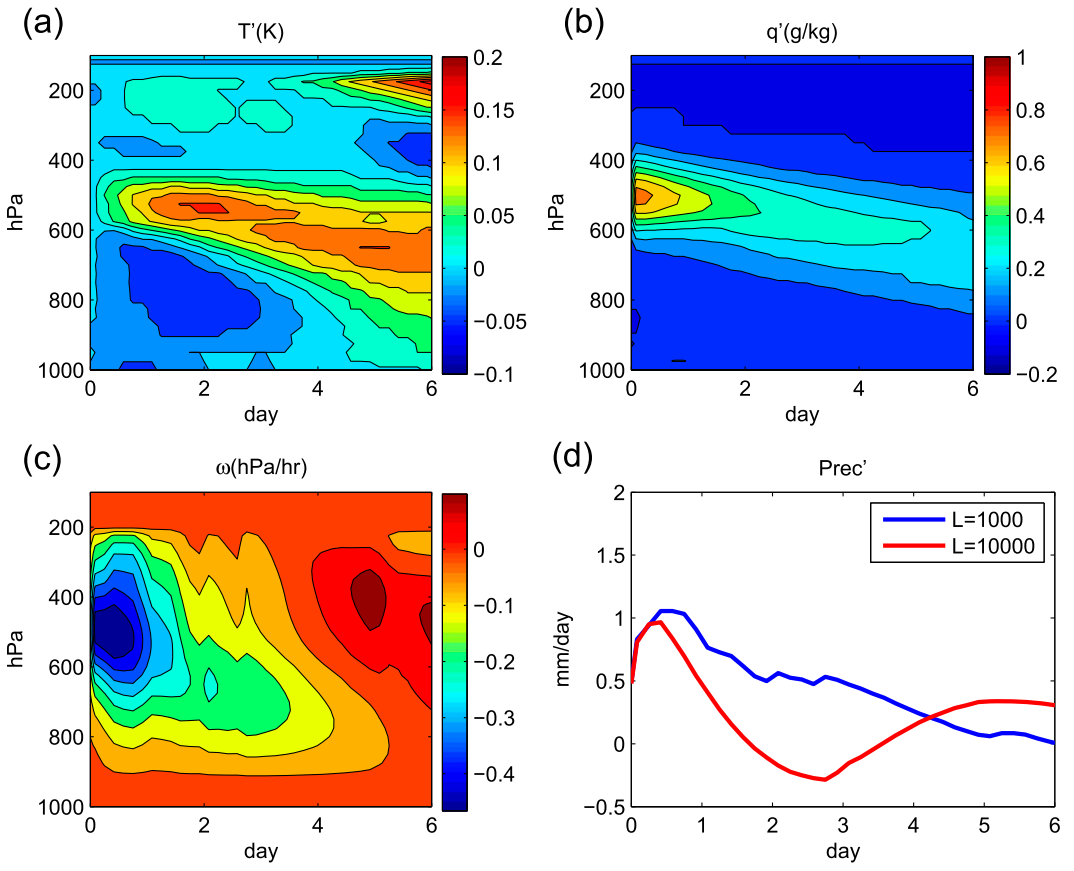

FIG. 4. As in Fig. 3, but using the SCM.

$$\partial_t T_m = \left(1 + \frac{\sigma k^2}{m^2 f_0^2}\right)^{-1} Q_m. \tag{9}$$

Although there are crude approximations in the derivation of Eqs. (8) and (9) and sinusoids are not eigenmodes of the system when the operator $Q(T, q)$ is included on the rhs, Eq. (9) reveals some basic properties of the system. As seen in Eq. (9), only a fraction $\{[1 + (\sigma k^2/m^2 f_0^2)]^{-1} < 1\}$ of the diabatic heating is converted into temperature tendency. The fraction decreases with smaller L (larger k), corresponding to slower adjustment. The physical interpretation aligns with the QG dynamics. Assuming there is some anomalous diabatic heating in an air column, under QG this air column cannot be warmed without correspondingly modifying the pressure field of its surrounding area. A fraction of the heating is used to reestablish the geostrophic and hydrostatic balance of the large-scale flow through vertical motion associated with ageostrophic winds. In the presence of a stable stratification, this vertical motion partly cancels the diabatic heating in the temperature equation, and the degree of the cancelation depends on the wavelength L. In the shortwave limit, the diabatic heating is totally canceled out, and the temperature tendency vanishes, which is consistent with the strict WTG approximation. Equation (9) also indicates that the vertical modes with smaller vertical wavenumbers (m) decay more slowly.

b. *Eigenanalysis of the linearized CQG system*

In this subsection, we go beyond the qualitative argument made with Eq. (9) to analyze the dynamics of the CQG system quantitatively, making use of the LRF. The LRF describes the dependencies of convective tendencies on the state vectors (T and q) by a linear matrix. We also discretize the QGω equation. Because both the LRF and the QGω equation are linear, they can be combined to form a single linear matrix equation that fully describes the CQG system.

With the convective tendencies calculated using the LRF [Eq. (6)], the temperature and moisture equations [Eqs. (1) and (2)] can be written as a matrix equation:

$$\begin{bmatrix} \partial_t T \\ \partial_t q \end{bmatrix} = \begin{bmatrix} \mathbf{M}_1 & \mathbf{M}_2 \\ \mathbf{M}_3 & \mathbf{M}_4 \end{bmatrix} \times \begin{bmatrix} T \\ q \end{bmatrix} + \begin{bmatrix} \dfrac{\sigma p}{R} \\ -s_q \end{bmatrix} \omega_Q. \tag{10}$$

Again, in this subsection we consider the case without horizontal advective forcing.

Next, we need to relate ω_Q to the state variables T and q, which is done through solving the QGω equation. The QGω equation can be solved using the Green's functions method. Let there be Green's functions $\hat{G}$ that satisfy

$$\partial_{pp}\hat{G} - \sigma\left(\frac{k}{f_0}\right)^2 \hat{G} = \delta(p - p'), \tag{11}$$

where δ is the Dirac delta function, and $\hat{G}$ has an analytical form for constant σ.[1] The term ω_Q is the integration of the Green's functions timing the convective heating term

$$\omega_Q(p) = \int_0^{p'} \left[\hat{G}(p,p')\frac{R}{p'}\left(\frac{k}{f_0}\right)^2 Q\right] dp'. \tag{12}$$

In the discretized form, the Green's functions $\hat{G}$ correspond to a Green's function matrix $\mathbf{G}$, which can be solved numerically for varying σ. Absorbing the coefficient R/p' into $\mathbf{G}$ and replacing Q using the LRF [Eq. (6)], one has

$$\omega_Q = \left(\frac{k}{f_0}\right)^2 [\mathbf{GM}_1 \quad \mathbf{GM}_2] \times \begin{bmatrix} T \\ q \end{bmatrix}. \tag{13}$$

Combining Eqs. (13) and (10), we have a new matrix equation that relates the tendencies of state vectors (T and q) to the state-vector anomalies, taking the coupling with QGω equation into account:

$$\begin{bmatrix} \partial_t T \\ \partial_t q \end{bmatrix} = \begin{bmatrix} \mathbf{M}_1 + \dfrac{\sigma p}{R}\left(\dfrac{k}{f_0}\right)^2 \mathbf{GM}_1 & \mathbf{M}_2 + \dfrac{\sigma p}{R}\left(\dfrac{k}{f_0}\right)^2 \mathbf{GM}_2 \\ \mathbf{M}_3 - s_q\left(\dfrac{k}{f_0}\right)^2 \mathbf{GM}_1 & \mathbf{M}_4 - s_q\left(\dfrac{k}{f_0}\right)^2 \mathbf{GM}_2 \end{bmatrix} \times \begin{bmatrix} T \\ q \end{bmatrix}. \tag{14}$$

[1] With boundary conditions of $\hat{G}(p_1) = 0$ and $\hat{G}(p_2) = 0$ ($p_2 > p_1$), and denoting $b^2 = \sigma(k/f_0)^2$, the analytical solution of Eq. (11) is

$$\hat{G}(p,p') = \frac{e^{-b(p+p_1)}}{2b(e^{2bp_1} - e^{2bp_2})} \times \begin{cases} e^{2b(p'+p_1)} + e^{2b(p+p_2)} - e^{2b(p+p')} - e^{2b(p_1+p_2)}, & \text{if} \quad p \le p' \\ e^{2b(p+p_1)} + e^{2b(p'+p_2)} - e^{2b(p+p')} - e^{2b(p_1+p_2)}, & \text{if} \quad p > p' \end{cases}.$$

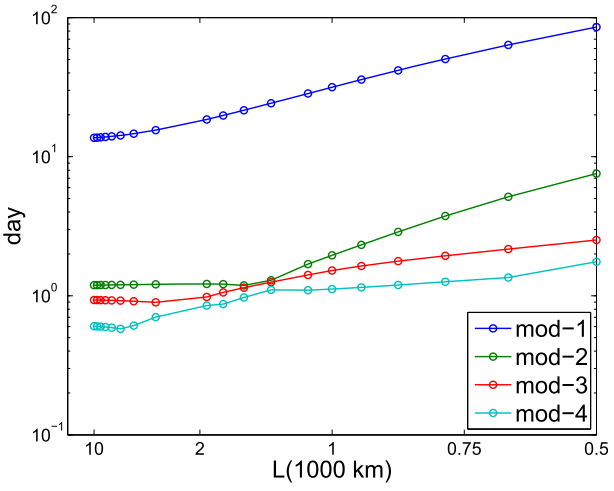

FIG. 5. The e-folding decay time of the first four eigenmodes of the linearized CQG system [Eq. (14)]. The eigenmodes are sequenced so that a slower-decaying mode has a smaller mode number. The x axis is the wavelength L with units of 1000 km.

Denoting the new matrix by $\mathbf{N}$ and the state vector by $\mathbf{X}$, given an initial value X_0, the time evolution of $\mathbf{X}$ is simply

$$\mathbf{X}(t) = e^{\mathbf{N}t} X_0. \tag{15}$$

If $\mathbf{X}$ happens to be the eigenvector of the matrix $\mathbf{N}$, we have

$$\mathbf{X}_n(t) = e^{\lambda_n t}\mathbf{X}_n, \tag{16}$$

where $\mathbf{X}_n$ is the nth eigenvector and λ_n is the corresponding eigenvalue. The term λ_n is the growth rate of the eigenmode. If the real part of λ_n is negative, as it is for all cases studied here, then Eq. (16) represents exponentially decaying solutions, with e-folding decay time λ_n^{-1}.

The matrix Eq. (14) fully describes the dynamics of the CQG system. Figure 5 shows the e-folding decay time of the first four eigenmodes of matrix $\mathbf{N}$ as functions of L. For the decoupled convection (L = 10 000 km, the leftmost dots in Fig. 5), the eigenmode decaying slowest has a decay time of about 15 days, while the rest of the eigenmodes have much shorter decay time (less than 2 days), consistent with the results in Kuang (2010, their Fig. 14). As L decreases, the decay times of all the eigenmodes increase, consistent with the results in section 4a and the qualitative argument leading to Eq. (9).

A longer decay time means that the system is less stable. The results above thus show that coupling with the large-scale ω destabilizes the system. The increases of the decay time with decreasing L are strongest for the

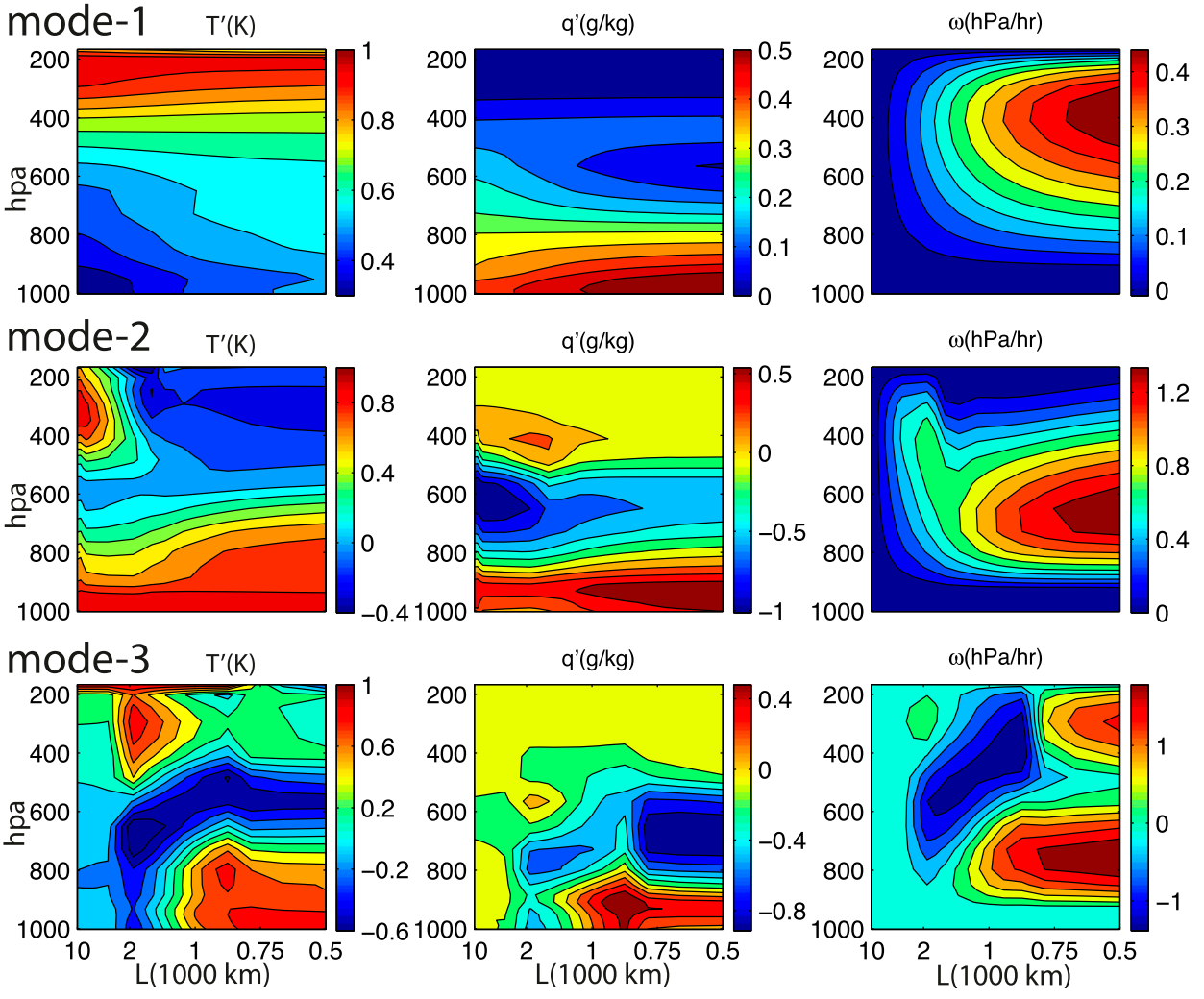

FIG. 6. The eigenvectors of (left) temperature, (center) specific humidity, and (right) ω as functions of wavelength L for (top) first, (middle) second, and (bottom) third eigenmodes. The eigenvectors are rescaled so that the temperature eigenvector has a maximum absolute value of +1 K.

first two eigenmodes (Fig. 5). For the higher eigenmodes, the decay time is still less than 2 days even when L is very small (e.g., $L = 500$ km). Thus, the first two eigenmodes, the least stable ones, largely explain the response of the CQG system after 2 days.

In Fig. 6, we show the vertical structures of the first three eigenmodes of matrix **N** for L ranging from 10 000 to 500 km. Because the system is linear, the signs and amplitudes of the eigenvectors are arbitrary. Here we rescale the eigenvectors so that the maximum absolute values of the T eigenvectors are +1 K. Also plotted is the structure of ω associated with each eigenvector. The following discussion is based on the rescaled eigenvectors. Let us first examine the first eigenmode (first row in Fig. 6). In the longwave limit (e.g., $L = 10\,000$ km), ω is close to zero as expected. The temperature and moisture eigenvectors are very close to the results in Kuang (2010, their Fig. 15). Kuang (2010) interprets this mode as a shift of the temperature profile to a warmer state following a moist adiabat with fixed relative humidity. The e-folding time scale (~15 days as seen in Fig. 5) is roughly the time needed for the anomalous surface flux to remove the column-integrated moist static energy anomaly associated with this eigenmode. As L decreases, a downward (positive) ω in the upper troposphere develops (top-right panel in Fig. 6) as a result of the anomalous diabatic cooling (i.e., reduced convective heating) associated with the warm temperature anomaly. The adiabatic warming caused by the descending motion partly cancels this convective cooling, consistent with the increased damping time of this eigenmode. The descending motion also accounts for the

midtropospheric drying in the moisture eigenvector (top-center panel in Fig. 6) and warming in the temperature eigenvector (top-center panel in Fig. 6) with small L. In the PBL and the lower troposphere where ω is small, specific humidity increases following the increases of temperature, presumably because relative humidity cannot change much there.

Next, we focus on the second eigenmode, shown in the middle row of Fig. 6. For the decoupled convection, both the temperature and moisture eigenvectors show negative anomalies in the middle troposphere and positive anomalies below and above. As L decreases to values smaller than 2000 km, the coupling between convection and ω alters the structure of the eigenmode. The temperature eigenvectors decrease with height to negative anomalies in the upper troposphere. The moisture eigenvectors are positive in the PBL and negative in the middle troposphere. The associated ω is a bottom-heavy ω profile with a single maximum near 700 hPa.

The third eigenmode shows even stronger dependencies on L than do the first two eigenmodes. The decoupled case has an upper-tropospheric warm anomaly. The weak convective adjustment in the upper troposphere leads to the relatively long damping time. With L between 2000 and 800 km, the temperature eigenvectors and ω show structures that change sign once with height. These profiles shift upward as L decreases. When L is smaller than 800 km, the middle troposphere becomes significantly dryer, and the upper-tropospheric ω changes sign to become positive.

The eigenvectors and their dependencies on L of other eigenmodes are also examined. Those eigenvectors show, for the most part, complex vertical structures and very strong dependencies on L. However, they share some common features, which already can be seen from Fig. 6. Generally, ω becomes significant and the eigenvectors change to structures different from those of the uncoupled system at around $L = 2000$ km, indicating that 2000 km is the wavelength that approximately separates decoupled and coupled convection. Not coincidentally, 2000 km is approximately the value of the deformation radius for our choices of parameters. As L decreases further, the eigenmodes approach the shortwave limit. Moreover, eigenvectors of higher eigenmodes have smaller vertical length scales, which is again consistent with Eq. (9). As shown in Fig. 5, the first two eigenmodes have significantly longer decay time, while the other eigenmodes decay more rapidly (2 days or less).

c. *Responses to transient forcing*

In this subsection, we examine the responses of the CQG system to transient large-scale forcing. We think of these calculations as representing an air column in the extratropical regions that is subjected to synoptic-scale disturbances, expressed through the large-scale advection terms (Adv_ζ, Adv_T, and Adv_q) in the CQG framework.

One straightforward approach would be to force the system with the advective forcing. However, as can be seen from Eq. (5), given the same Adv_ζ or Adv_T, the corresponding ω_ζ or ω_T also depends on wavelength L. Thus, with the same Adv_ζ forcing, for example, the differences of the responses come from both the dependence of ω_ζ and the strength of coupling between convection and large-scale vertical motion on L. Given the above reasoning, we choose to force the system by an imposed component of ω itself, so that the dependence of the response on L is only due to the strength of coupling. We also separate the dynamical and thermodynamical effects of Adv_T. The new set of forcings then consists of a dynamical forcing ω_d, which is due either to Adv_ζ, Adv_T, or a combination of the two; temperature forcing Adv_T, but applied only in the temperature equation; and moisture forcing Adv_q applied in the moisture equation as before. The forcings are Gaussian shaped in pressure with a standard deviation of 75 hPa. The amplitudes are $-0.5\,\mathrm{hPa\,h^{-1}}$ for ω_d, $-0.5\,\mathrm{K\,day^{-1}}$ for Adv_T, and $0.5\,\mathrm{g\,kg^{-1}\,day^{-1}}$ for Adv_q. The forcing is applied for 1 day to the initial RCE profiles, after which the system evolves unforced. We run simulations with each forcing applied on different tropospheric pressure levels over a range of wavelengths L. Only the results using the LRF are shown.

Before examining the overall features of the responses, we show the evolution of the $L = 1000$-km case with an ω_d forcing localized near 500 hPa as an example in Fig. 7. The imposed ω_d (Fig. 7d) adiabatically cools the middle troposphere (Fig. 7a) and encourages deep convection. The positive convective heating anomalies associated with the strengthened convection further induce an upward ω_Q (Fig. 7c), positively feeding back to the initially imposed upward ω. With $L = 1000$ km, the feedback (ω_Q) has a peak amplitude of about $-1.5\,\mathrm{hPa\,h^{-1}}$, about 3 times greater than the imposed forcing (ω_d) itself. There are positive q anomalies in the middle troposphere and negative q anomalies in the lower troposphere (Fig. 7c), broadly consistent with the dipole ω profiles initially. The precipitation anomaly linearly increases during the forcing period, then slowly decays with a time scale of several days (Fig. 7e). As a comparison, the precipitation anomaly to the same forcing but with $L = 10\,000$ km is plotted as the red line in Fig. 7e. Without the diabatic feedback, convection only passively responds to the imposed ω_d. The peak of precipitation anomaly is only one-third of the

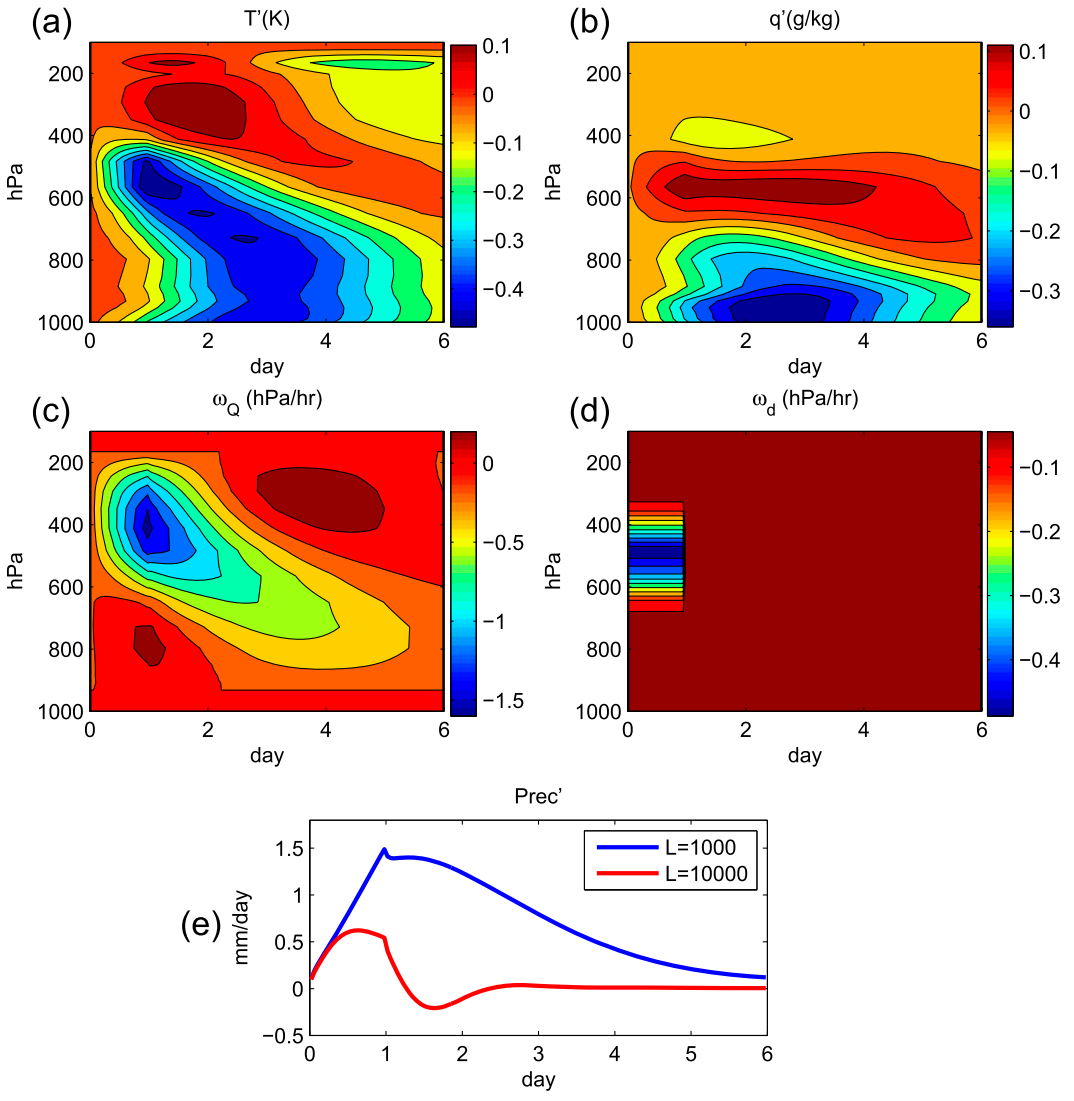

FIG. 7. Time series of (a) temperature, (b) specific humidity, (c) ω_Q, (d) ω_d, and (e) precipitation anomalies with an ω_d forcing centered at 500 hPa. These are the results using the LRF with $L = 1000$ km.

$L = 1000$-km case and decays quickly after the forcing stops.

The peak value of the precipitation anomaly, δP, within a relevant time (e.g., 6 days) is a basic metric by which we can characterize the responses of the CQG system to transient forcings. Figures 8a–c present this metric for each type of forcing applied at each pressure level (y axes) with different L (x axes). These figures serve as a lookup table; they tell us what the precipitation and, thus, what column-integrated convective heating occurs for a given forcing. In the linear regime, the precipitation response to an arbitrary combination of these forcings is the sum of the responses of the projections of the forcings onto the Gaussian bases.

We first examine δP for the temperature forcing in Fig. 8b. As a comparison, δP for the decoupled cases (i.e., $L = 10\,000$-km case) to the same temperature forcing is also shown in Fig. 8d as a function of the forcing level. For the decoupled cases, putting the transient cooling in the middle troposphere leads to a peak δP of about $0.5\,\text{mm day}^{-1}$, which corresponds closely to the convective heating anomaly that would be required to balance the imposed cooling in equilibrium. When cooling is applied in the upper or lower troposphere, δP is smaller, indicating that for those cases a forced equilibrium has not been reached yet after one day. As L decreases, the increasingly strong diabatic heating feedback leads to larger precipitation responses (Fig. 8b). There is a maximum region of δP for forcing

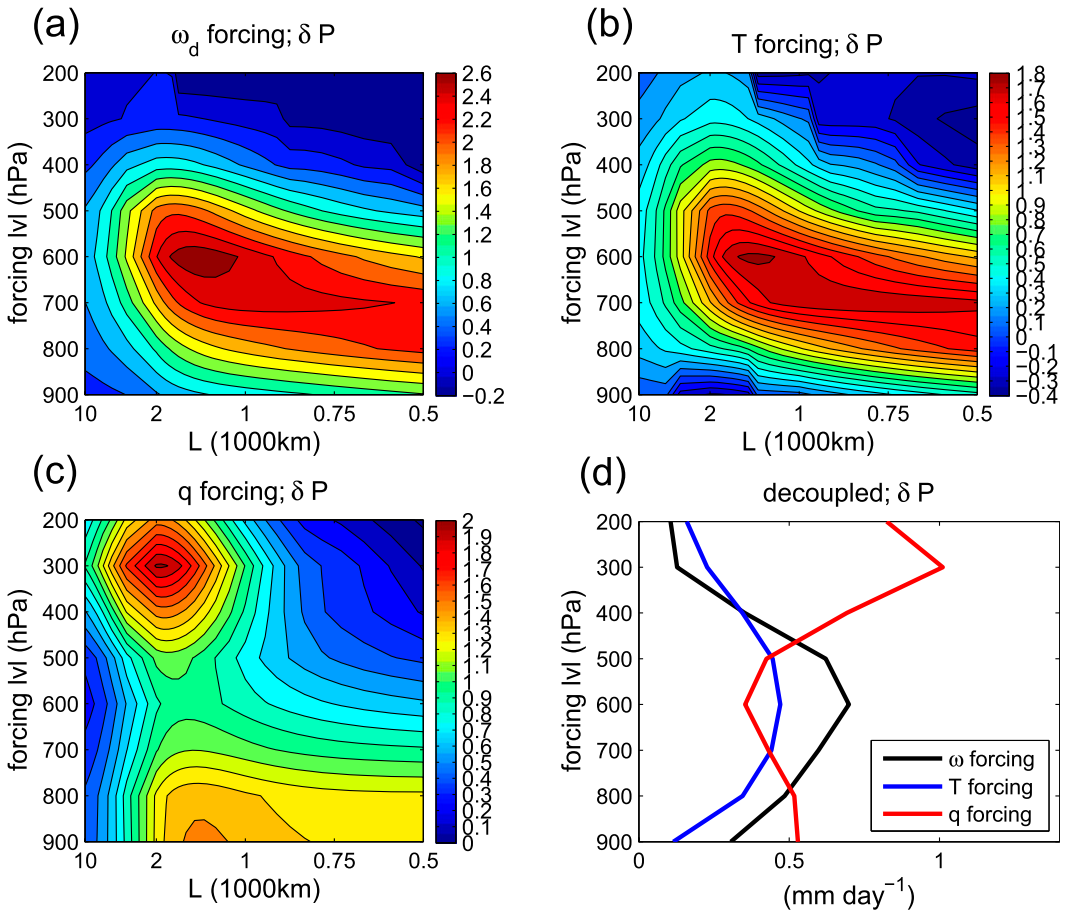

FIG. 8. The precipitation response maximum within 6 days (δP) when (a) ω_d, (b) temperature, and (c) moisture forcing is applied at each pressure level. The x axes are wavelength L, and y axes are the level at which the forcing is applied. (d) δP to the same set of forcing but with convection decoupled with QG ω.

between approximately 600 and 700 hPa and L between approximately 2000 and 1000 km. Over that region, the diabatic heating feedback increases the precipitation response by a factor of 4. As L further decreases, δP does not increase, but its maximum region slightly shifts downward to lower levels. Cooling the PBL temporarily inhibits convection and induces convective cooling anomalies and negative precipitation responses.

Contrarily, with decoupled convection, δP has a minimum for moisture forcing in the middle troposphere (red line in Fig. 8d). This is consistent with the characteristics of the LRF, which shows larger responses to moisture perturbations in the lower or upper troposphere (Fig. 8 in Kuang 2012). However, δP for upper-tropospheric moisture forcing does not represent the response to realistic perturbations. The LRF measures the response to a perturbation of constant magnitude in specific humidity while specific humidity anomalies in the real upper troposphere are limited to values much smaller than those below because of the much lower temperatures and saturation specific humidities. As L decreases, similarly, the diabatic heating feedback amplifies the responses. For lower-tropospheric moisture forcing, the amplification of δP maximizes at a factor of 2 to the decoupled case when L is between approximately 2000 and 1000 km. As L further decreases, δP actually slightly decreases for lower-level forcing and strongly decreases for upper-level forcing.

The pattern of the δP response to ω_d forcing (Fig. 8a) largely resembles that to temperature forcing (Fig. 8b). This is perhaps not surprising, as ω_d affects the system both through the associated diabatic heating and the vertical moisture transport and, thus, is equivalent to a combination of temperature and moisture forcings. The main differences between Figs. 8a and 8b are in the lower troposphere, where the response to ω_d forcing is more positive than that to temperature forcing. The vertical moisture transport by ω_d is significant there and modifies the precipitation response.

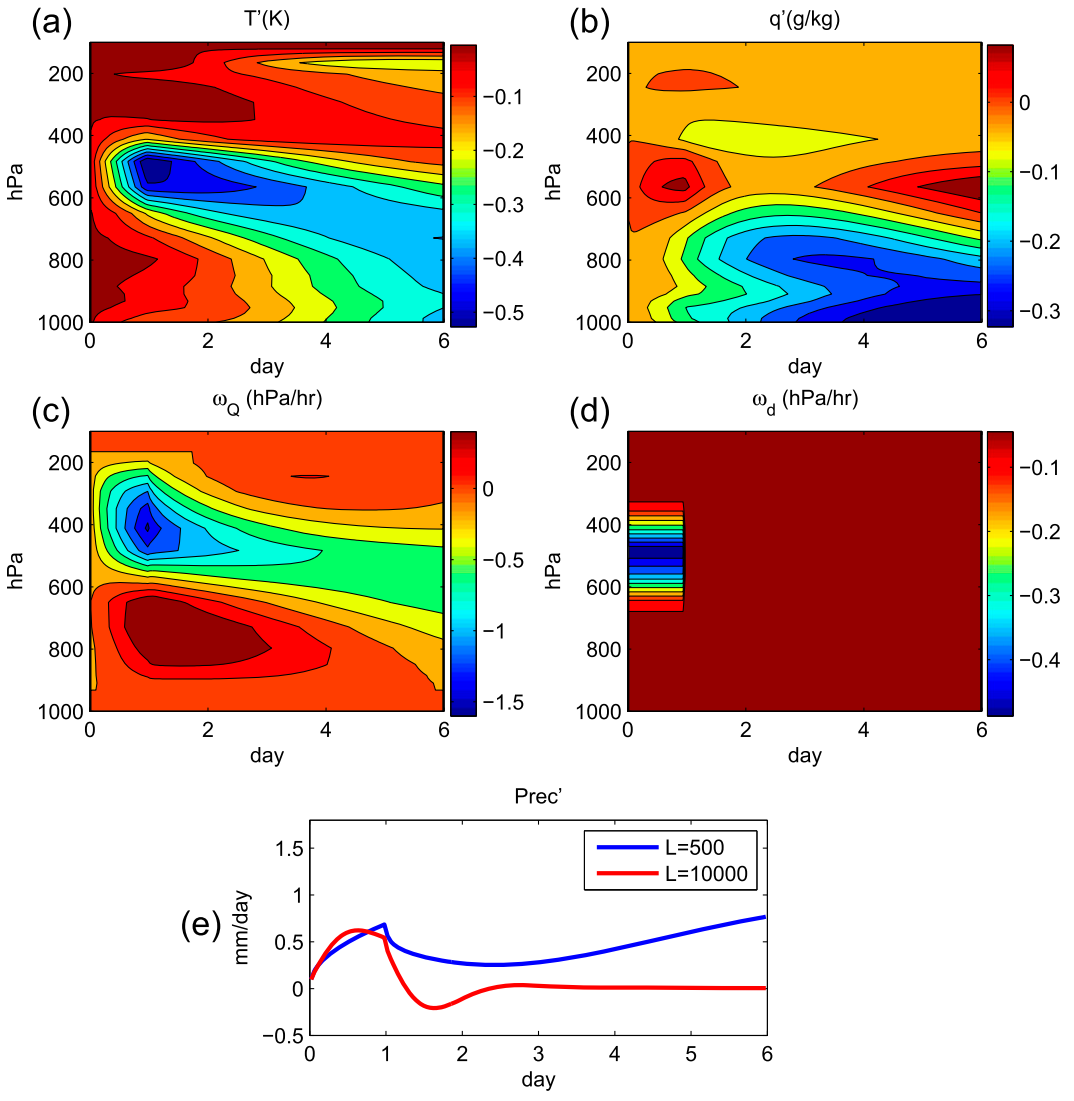

FIG. 9. As in Fig. 7, but with $L = 500$ km.

An intriguing feature seen in Figs. 8a–c is that peak regions of δP occurs with L between approximately 2000 and 1000 km. One might have expected that with even smaller L, the stronger coupling between convection and ω should lead to greater δP. Examining the simulations suggests the following reason why this is not the case: as L further decreases, for a given diabatic heating Q, the resulting ω_Q is more localized vertically. This can be explained in terms of the relative importance of the Laplacian operator ∂_{pp}, which is diffusive vertically, and the linear operator $-\sigma(k/f_0)^2$, which localizes the responses in the lhs of the QGω equation. When L is small, the latter dominates, localizing ω_Q to the region of convective heating anomalies. This usually leads to a dipole structure in ω_Q. To demonstrate this point, in Fig. 9, we show the responses to the same ω_d forcing as in Fig. 7, but with $L = 500$ km. The temperature anomalies and ω_Q persist locally in the vertical direction and do not effectively communicate with other levels. The term ω_Q clearly shows a dipole structure (Fig. 9c). The cancellation of the upward and downward motion of the dipole leads to smaller precipitation responses to the forcing (Fig. 9e).

In summary, after exploring the responses of convection in the CQG framework to a set of transient forcings that separate dynamics from thermodynamics, we find that the precipitation has the strongest responses to forcing in temperature when it acts in the middle troposphere and to moisture when it acts in the lower troposphere (discounting the hypothetical strong responses to the unrealistically large upper-tropospheric moisture forcing). The responses to dry QG ω forcing,

which can be further projected into the temperature and moisture forcings, resemble the responses to temperature forcing, but with additional modulation in the lower troposphere by moisture transport effects. The diabatic heating feedback of convection on ω is strongest when L is roughly between approximately 2000 and 1000 km. This optimal wavelength is a consequence of competition between the strength of the coupling between convection and ω and the vertical scale of the QG ω response, which depend in opposite senses on L.

5. Discussion

The QGω equation is six decades old [e.g., review of Davies (2015)], but has been used mainly as a diagnostic equation. The novelty of the current study is in using it in a predictive modeling framework to quantify the interaction between convection and large-scale dynamics in a single column. We suggest here a few possible applications.

In principle, this framework could allow us to attribute the precipitation of strong rainfall events to different large-scale forcings and the resulting convective feedback. We are interested particularly in subtropical precipitation extreme events, where the latitude is high enough that the quasigeostrophic dynamics is at least qualitatively relevant, while moisture may be abundant and convection strong. Prominent examples are events occurring in northern Pakistan during the summer monsoon seasons (e.g., Rasmussen et al. 2015). These extreme events are usually thought to be associated with upper-level advection of potential vorticity anomalies of extratropical origin, subtropical monsoon depressions, low-level moisture transport, and topographic upslope flow in some combination (e.g., Houze et al. 2011; Galarneau et al. 2012; Rasmussen and Houze 2012; Martius et al. 2013). Within the CQG modeling framework, the roles of these different factors can be decomposed into the corresponding advection terms. To the extent that the convective response can be accurately simulated within this framework (something that will depend both on the validity of the framework itself and the quality of the underlying model of convection), we can understand the role of each factor in determining the convective response.

Another potential application is to help understand the structure of convection in organized convective systems, such as monsoon depressions (e.g., Godbole 1977; Mooley and Shukla 1987; Hurley and Boos 2015). Observations show a dipole heating profile in the southwest quadrant of the monsoon depression vortex, which may contribute to the axial asymmetry of the vortex and its westward advection (Boos et al. 2015, 2016). One may imagine using the CQG modeling framework to examine what determines this structure by simulating a convective column in the southwest quarter forced by the advection associated with the monsoon depression vortex.

The CQG framework can also serve as a test bed for improving convective parameterizations. The performance of a convective parameterization is sometimes evaluated in single-column tests with imposed large-scale ω. These kinds of tests, however, may obscure the deficiencies of the convective parameterization by overconstraining the system. When adiabatic cooling due to large-scale vertical motion is imposed, in steady state (or even in a time-varying state, to the extent that temperature changes are small compared to heating terms) any convective parameterization has to produce the same amount of convective heating to balance the imposed cooling. Raymond (2007) tested a convective parameterization against a CRM in a modeling framework with parameterized large-scale dynamics—in that case, the WTG framework for the tropics. Indeed, recent model intercomparison studies (Daleu et al. 2015, manuscript submitted to *J. Adv. Model. Earth Syst.*, 2015) showed that different convective parameterizations had a wide range of behaviors under the same conditions with WTG implemented. Similarly, comparing how convection interacts with large-scale dynamics in the CQG framework with convection represented by convective parameterizations and CRMs may better identify the deficiencies of convective parameterizations and guide their improvement.

The CQG framework has significant limitations, in addition to those associated with the quasigeostrophic approximation itself. Using the QGω equation, we parameterize the interaction between convective heating and large-scale dynamics in a single column. However, convective heating also causes changes to the horizontal structures of the temperature and wind fields on large scales, which can be expected to alter the horizontal advective forcings acting on the convective column. These feedbacks are not included in this framework, since the horizontal advection terms are treated as given. The consequences of this limitation, or the extent to which it can be overcome by additional parameterizations, are not addressed here. Our initial experiments in simulating a couple of extreme precipitation events (to be reported in due time), however, suggest that the CQG framework as proposed here is adequate to provide useful insights into the dynamics of the events in question, suggesting that it may have broader usefulness despite its limitations.

In the present study, we have focused on the interaction between convection and QG vertical motion in the linear regime. However, the CQG framework itself does

not assume linearity. Although the QG omega equation is linear for specified forcings, the dependencies of convection on the state variables can be nonlinear for large perturbations. In this case, our results here with the LRF will not provide a complete description of the relevant dynamics. The nonlinearities can be explored with SCMs or CRMs in the CQG framework.

6. Conclusions

Extending the concept of parameterization of large-scale dynamics developed in tropical meteorology, we propose a framework that allows interactions between convection and large-scale quasigeostrophic dynamics in a single column. The framework parameterizes the large-scale vertical motion using the QG omega equation. Convective processes are represented by a single-column model or a limited domain cloud-resolving model. The vertical motion modifies the thermodynamical profiles of the convective column by the associated adiabatic cooling and vertical transport of moisture, while in turn being modified by the diabatic heating associated with convection.

The strength of the coupling between convection and vertical motion is set by the characteristic wavelength of the disturbance. Strong coupling with vertical motion reduces the stability of the system, so that the responses persist for a longer time period and with greater amplitude compared to the case of decoupled convection. The eigenmodes of the linearized system show a regime transition as the wavelength decreases from infinity to several hundred kilometers. When forced by transient forcing, the amplification of the precipitation response due to the coupling of convection and vertical motion can be as large as a factor of 4, depending on the wavelength and vertical structure of the forcing. The strongest responses are to middle-troposphere temperature forcing and to lower-troposphere moisture forcing. The diabatic feedback of convection on vertical motion is strongest for wavelengths on the order of the Rossby deformation radius, here roughly between 2000 and 1000 km. When L is smaller than that, the diabatically forced vertical motion is trapped locally in the vertical, leading to smaller responses in precipitation. We argue that this modeling framework can be a useful tool to study the interaction between convection and large-scale dynamics from the single-column point of view.

Acknowledgments. The authors thank Daniel Shaevitz, Shuguang Wang, Zhiming Kuang for discussion, Zhiming Kuang for providing the linear response functions, and Brian Mapes and two anonymous reviewers for their helpful reviews. The authors also wish to acknowledge Michael Herman's generosity for providing another set of linear response functions, even though it was not eventually used in this paper. This research was supported by the Lamont Postdoctoral Fellowship to JN and an AXA Award from the AXA Research Fund to AHS.

REFERENCES

Bergman, J. W., and P. D. Sardeshmukh, 2004: Dynamic stabilization of atmospheric single column models. *J. Climate*, **17**, 1004–1021, doi:10.1175/1520-0442(2004)017<1004:DSOASC>2.0.CO;2.

Blossey, P. N., C. S. Bretherton, and M. C. Wyant, 2009: Understanding subtropical low cloud response to a warmer climate in a superparameterized climate model. Part II: Column modeling with a cloud-resolving model. *J. Adv. Model. Earth Syst.*, **1** (8), doi:10.3894/JAMES.2009.1.8.

Bony, S., and K. A. Emanuel, 2001: A parameterization of the cloudiness associated with cumulus convection: Evaluation using TOGA COARE data. *J. Atmos. Sci.*, **58**, 3158–3183, doi:10.1175/1520-0469(2001)058<3158:APOTCA>2.0.CO;2.

Boos, W. R., J. V. Hurley, and V. S. Murthy, 2015: Adiabatic westward drift of Indian monsoon depressions. *Quart. J. Roy. Meteor. Soc.*, **141**, 1035–1048, doi:10.1002/qj.2454.

——, B. E. Mapes, and V. S. Murthy, 2016: Potential vorticity structure and propagation mechanism of Indian monsoon depressions. *The Global Monsoon System*, C.P. Chang et al., Eds., World Scientific Series on Asia-Pacific Weather and Climate, World Scientific, in press.

Charney, J. G., 1963: A note on large-scale motions in the tropics. *J. Atmos. Sci.*, **20**, 607–609, doi:10.1175/1520-0469(1963)020<0607:ANOLSM>2.0.CO;2.

Chiang, J. C. H., and A. H. Sobel, 2002: Tropical tropospheric temperature variations caused by ENSO and their influence on the remote tropical climate. *J. Climate*, **15**, 2616–2631, doi:10.1175/1520-0442(2002)015<2616:TTTVCB>2.0.CO;2.

Daleu, C. L., and Coauthors, 2015: Intercomparison of methods of coupling between convection and large-scale circulation: 1. Comparison over uniform surface conditions. *J. Adv. Model. Earth Syst.*, **7**, 1576–1601, doi:10.1002/2015MS000468.

Davies, H. C., 2015: The quasigeostrophic omega equation: Reappraisal, refinements, and relevance. *Mon. Wea. Rev.*, **143**, 3–25, doi:10.1175/MWR-D-14-00098.1.

Emanuel, K. A., 1991: A scheme for representing cumulus convection in large-scale models. *J. Atmos. Sci.*, **48**, 2313–2335, doi:10.1175/1520-0469(1991)048<2313:ASFRCC>2.0.CO;2.

——, and M. Živkovic-Rothman, 1999: Development and evaluation of a convection scheme for use in climate models. *J. Atmos. Sci.*, **56**, 1766–1782, doi:10.1175/1520-0469(1999)056<1766:DAEOAC>2.0.CO;2.

——, A. A. Wing, and E. M. Vincent, 2014: Radiative-convective instability. *J. Adv. Model. Earth Syst.*, **6**, 75–90, doi:10.1002/2013MS000270.

Galarneau, T. J., Jr., T. M. Hamill, R. M. Dole, and J. Perlwitz, 2012: A multiscale analysis of the extreme weather events over western Russia and northern Pakistan during July 2010. *Mon. Wea. Rev.*, **140**, 1639–1664, doi:10.1175/MWR-D-11-00191.1.

Godbole, R. V., 1977: Composite structure of monsoon depression. *Tellus*, **29A**, 25–40, doi:10.1111/j.2153-3490.1977.tb00706.x.

Herman, M. J., and Z. Kuang, 2013: Linear response functions of two convective parameterization schemes. *J. Adv. Model. Earth Syst.*, **5**, 510–541, doi:10.1002/jame.20037.

Holton, J., 2004: *An Introduction to Dynamic Meteorology*. 4th ed. Academic Press, 535 pp.

Hoskins, B. J., I. Draghici, and H. C. Davies, 1978: A new look at the ω-equation. *Quart. J. Roy. Meteor. Soc.*, **104**, 31–38, doi:10.1002/qj.49710443903.

——, I. N. James, and G. H. White, 1983: The shape, propagation and mean-flow interaction of large-scale weather systems. *J. Atmos. Sci.*, **40**, 1595–1612, doi:10.1175/1520-0469(1983)040<1595:TSPAMF>2.0.CO;2.

Houze, R. A., Jr., K. L. Rasmussen, S. Medina, S. R. Brodzik, and U. Romatschke, 2011: Anomalous atmospheric events leading to the summer 2010 floods in Pakistan. *Bull. Amer. Meteor. Soc.*, **92**, 291–298, doi:10.1175/2010BAMS3173.1.

Hurley, J. V., and W. R. Boos, 2015: A global climatology of monsoon low-pressure systems. *Quart. J. Roy. Meteor. Soc.*, **141**, 1049–1064, doi:10.1002/qj.2447.

Kuang, Z., 2008: Modeling the interaction between cumulus convection and linear waves using a limited domain cloud system–resolving model. *J. Atmos. Sci.*, **65**, 576–591, doi:10.1175/2007JAS2399.1.

——, 2010: Linear response functions of a cumulus ensemble to temperature and moisture perturbations and implication to the dynamics of convectively coupled waves. *J. Atmos. Sci.*, **67**, 941–962, doi:10.1175/2009JAS3260.1.

——, 2012: Weakly forced mock Walker cells. *J. Atmos. Sci.*, **69**, 2759–2786, doi:10.1175/JAS-D-11-0307.1.

Mapes, B. E., 2004: Sensitivities of cumulus ensemble rainfall in a cloud-resolving model with parameterized large-scale dynamics. *J. Atmos. Sci.*, **61**, 2308–2317, doi:10.1175/1520-0469(2004)061<2308:SOCRIA>2.0.CO;2.

Martius, O., and Coauthors, 2013: The role of upper-level dynamics and surface processes for the Pakistan flood of July 2010. *Quart. J. Roy. Meteor. Soc.*, **139**, 1780–1797, doi:10.1002/qj.2082.

Mooley, D. A., and J. Shukla, 1987: Characteristics of the westward moving summer monsoon low-pressure systems over the Indian region and their relationship with the monsoon rainfall. Center for Ocean–Land–Atmosphere Interactions Tech. Rep., 218 pp. [Available online at http://www.iges.org/people/Shukla's%20Articles/1988/Characteristics.pdf.]

Nie, J., and Z. Kuang, 2012a: Responses of shallow cumulus convection to large-scale temperature and moisture perturbations: A comparison of large-eddy simulations and a convective parameterization based on stochastically entraining parcels. *J. Atmos. Sci.*, **69**, 1936–1956, doi:10.1175/JAS-D-11-0279.1.

——, and ——, 2012b: Beyond bulk entrainment and detrainment rates: A new framework for diagnosing mixing in cumulus convection. *Geophys. Res. Lett.*, **39**, L21803, doi:10.1029/2012GL053992.

——, and A. H. Sobel, 2015: Responses of tropical deep convection to the QBO: Cloud-resolving simulations. *J. Atmos. Sci.*, **72**, 3625–3638, doi:10.1175/JAS-D-15-0035.1.

Pauluis, O., and S. Garner, 2006: Sensitivity of radiative–convective equilibrium simulations to horizontal resolution. *J. Atmos. Sci.*, **63**, 1910–1923, doi:10.1175/JAS3705.1.

Rasmussen, K. L., and R. A. Houze, 2012: A flash-flooding storm at the steep edge of high terrain: Disaster in the Himalayas. *Bull. Amer. Meteor. Soc.*, **93**, 1713–1724, doi:10.1175/BAMS-D-11-00236.1.

——, A. J. Hill, V. E. Toma, M. D. Zuluaga, P. J. Webster, and R. A. Houze, 2015: Multiscale analysis of three consecutive years of anomalous flooding in Pakistan. *Quart. J. Roy. Meteor. Soc.*, **141**, 1259–1276, doi:10.1002/qj.2433.

Raymond, D. J., 2007: Testing a cumulus parametrization with a cumulus ensemble model in weak-temperature-gradient mode. *Quart. J. Roy. Meteor. Soc.*, **133**, 1073–1085, doi:10.1002/qj.80.

——, and X. Zeng, 2005: Modelling tropical atmospheric convection in the context of the weak temperature gradient approximation. *Quart. J. Roy. Meteor. Soc.*, **131**, 1301–1320, doi:10.1256/qj.03.97.

Romps, D. M., 2012a: Weak pressure gradient approximation and its analytical solutions. *J. Atmos. Sci.*, **69**, 2835–2845, doi:10.1175/JAS-D-11-0336.1.

——, 2012b: Numerical tests of the weak pressure gradient approximation. *J. Atmos. Sci.*, **69**, 2846–2856, doi:10.1175/JAS-D-11-0337.1.

Sobel, A. H., and C. S. Bretherton, 2000: Modeling tropical precipitation in a single column. *J. Climate*, **13**, 4378–4392, doi:10.1175/1520-0442(2000)013<4378:MTPIAS>2.0.CO;2.

——, J. Nilsson, and L. M. Polvani, 2001: The weak temperature gradient approximation and balanced tropical moisture waves. *J. Atmos. Sci.*, **58**, 3650–3665, doi:10.1175/1520-0469(2001)058<3650:TWTGAA>2.0.CO;2.

——, G. Bellon, and J. Bacmeister, 2007: Multiple equilibria in a single-column model of the tropical atmosphere. *Geophys. Res. Lett.*, **34**, L22804, doi:10.1029/2007GL031320.

Trenberth, K. E., 1978: Interpretation of the diagnostic quasi-geostrophic omega equation. *Mon. Wea. Rev.*, **106**, 131–137, doi:10.1175/1520-0493(1978)106<0131:OTIOTD>2.0.CO;2.

Tulich, S. N., and B. E. Mapes, 2010: Transient environmental sensitivities of explicitly simulated tropical convection. *J. Atmos. Sci.*, **67**, 923–940, doi:10.1175/2009JAS3277.1.

Wang, S., and A. H. Sobel, 2011: Response of convection to relative sea surface temperature: Cloud-resolving simulations in two and three dimensions. *J. Geophys. Res.*, **116**, D11119, doi:10.1029/2010JD015347.